Numerical solution of time-dependent Schrödinger equation for multiphoton processes: A matrix iterative method

M. Nurhuda[1,2] and F. H. M. Faisal[1,*]
[1]*Fakultät für Physik, Universität Bielefeld, Postfach 100131, D-33501 Bielefeld, Germany*
[2]*Physics Department, Brawijaya University, Malang 65144, Indonesia*
(Received 30 March 1999)

An implicit algorithm for integration of the three-dimensional (3D) time-dependent Schrödinger equation of an atomic system interacting with intense laser pulses is developed. It is based on a matrix iteration of the Crank-Nicholson approximant to the short-time propagator using the *total* Hamiltonian (unsplit) of the system directly. To test the method, 3D Schrödinger wave-packet propagation is carried out, and so-called above-threshold ionization and high-harmonic generation spectra for atomic hydrogen irradiated by intense laser pulses are obtained. They are also compared with that obtained using the popular split-operator method. The present algorithm is shown to provide an alternative to the the split-operator method, and proves to be more efficient in all the cases studied here. A procedure for optimizing the maximum grid size is also given, and its usefulness is illustrated. [S1050-2947(99)06409-4]

PACS number(s): 32.80.Rm, 32.80.Fb, 42.65.Ky

I. INTRODUCTION

Interaction of intense laser pulses with atomic systems has been a subject of much experimental and theoretical interest since the discovery of such highly nonlinear and yet ubiquitous phenomena as the so-called above-threshold ionization (ATI) [1,2] and high-harmonic generation (HHG) [3,4]. The ATI process is characterized by a sequence of peaks in the energy spectrum of ejected electrons, that are separated by the photon energy of the laser, while in the HHG process an entire spectrum of coherent radiation is emitted at frequencies characterized by odd multiples of the incident laser frequency. In experiments, harmonics well above 100 have been observed [5,6]. This has stimulated great interest in view of the possibility of generating a coherent source of radiation in the vaccum ultraviolet and the soft-x-ray domains [7,8]. Theoretical investigations of such highly nonlinear processes require a direct integration of the time-dependent Schrödinger equation (TDSE), that was initiated in the late 1980s [9], and continued vigorously since then [10].

One of the popular methods for propagating the solution of the TDSE has been the so-called split-operator method [11–13], in which the total Hamiltonian operator is separated into a sum of two terms; the reference Hamiltonian H_0, and the interaction Hamiltonian $H_{\rm int}$; the short-time propagation is given in the form

$$\Psi(\mathbf{r},t+\Delta t)\approx e^{-iH_0\Delta t/2}e^{-iH_{int}\Delta t/2}e^{-iH_0\Delta t/2}\Psi(\mathbf{r},t). \quad (1)$$

The error term in this propagator, $O(\Delta t)^3$, is of the third order in Δt, with coefficients depending on the nonvanishing second-order commutator between the unperturbed Hamiltonian and the interaction Hamiltonian [cf. Eq. (22) below]. The method is thus efficient when the error arising from the noncommutation between H_0 and $H_{\rm int}$ is small. For a given Δt, this error, however, behaves differently depending on the radial distance r and the choice of the gauge of the interaction. Thus, in the length gauge, simulations are most effective when the electronic wave packet during the time evolution does not move too far away from the nucleus at the origin, e.g., when the pulse duration is very short or the laser intensity is moderately weak. For moderately long and strong fields, electron-field interaction can cause so-called ''wave-packet explosion,'' i.e., the wave packet propagates very rapidly away from the nucleus and the computation may fail to converge within a managable grid size. This awkward situation is often avoidable by using the interaction Hamiltonian in the so-called velocity gauge [14]. Unfortunately, the split-operator method applied to the interaction in the velocity gauge can cause the second-order commutation error (for a given size of Δt) to be large at small radial distances (for details see Sec. III below). Note also that the splitting of the short-time propagator in Eq. (1) requires in general a triple matrix product operations per unit time step, and/or it has to be combined with fast Fourier transform (FFT) techniques [11].

The above considerations suggest that it might be profitable to consider an algorithm which deals directly with the total Hamiltonian in the short-time propagator or its Crank-Nicholson approximant, since this might help in reducing both the noncommutation error and avoid the triple-matrix product and/or FFT of the short-time propagator in the split-operator form. The purpose of this paper is to present such a method and show its usefulness by application to Schrödinger wave-packet propagation in three dimension. The efficacy of the method for real problems is shown by applying it to the problems of computing the ATI and HHG spectra for hydrogen atom in intense laser pulses, and for both high and low carrier frequencies.

The rest of the paper is organized as follows: Sec. II deals with the formal derivation of the algorithm of the present method, referred to below as the ''matrix iterative method'' (for reasons that will be apparent shortly). In Sec. III, using the simulated wave packets, the spectra of both ATI and HHG processes are computed. Similar simulations and computations of the spectra are carried out using the split-

*Electronic address:ffaisal@physik.uni-bielefeld.de

operator method as well. The results obtained by the two methods are compared. Comparisons are made in two regimes of laser frequency, i.e., for frequencies both higher and lower than the Bohr frequency of the target atom. In Sec. IV, a method for optimizing the grid size is presented. Finally, in Sec. V, results are summarized and short remarks on further prospects of the algorithm are made.

II. BASIC THEORY AND ALGORITHM

The Schrödinger equation governing the atom-field interaction can be written as (we use, unless explicitly given otherwise, Hartree atomic units $e=m=\hbar=1$ and $c\approx 137$)

$$i\frac{\partial}{\partial t}\Psi(\mathbf{r},t)=(H_0+H_{\rm int})\Psi(\mathbf{r},t), \tag{2}$$

where H_0 is the unperturbed atomic Hamiltonian, and $H_{\rm int}$ is the interaction Hamiltonian. The solution of Eq. (2) at a time $t+\Delta t$ is connected to the solution at t by a short-time propagator that can be written using the full Hamiltonian, in contradiction to Eq. (1), as

$$\Psi(\mathbf{r},t+\Delta t)\approx e^{-iH\Delta t}\Psi(\mathbf{r},t). \tag{3}$$

The Crank-Nicholson approximant of the short-time propagator (3) can be expressed as [15,16]

$$\Psi(\mathbf{r},t+\Delta t)=\frac{1-iH\Delta t/2}{1+iH\Delta t/2}\Psi(\mathbf{r},t)+\frac{1}{4}(H\Delta t)^3. \tag{4}$$

Unfortunately, scheme (4) requests an inversion of the matrix representation of $(1+iH\Delta t/2)$, which can be very demanding for a problem involving more than one dimension [11]. In order to avoid such matrix inversions, we introduce a matrix iterative method below. We may begin by expanding the total wave function in a discrete set of orthonormal basis functions (on which the total Hamiltonian can be given a matrix operator representation) as

$$\Psi(\mathbf{r},t)=\sum_k b_k(\xi_1,t)P_k(\xi_2), \tag{5}$$

where $P_k(\xi_2)$ stands for the basis function in the set of variables ξ_2, and $b_k(\xi_1,t)$ is the corresponding time-dependent coefficient of expansion in a continuous variable ξ_1. The left-hand side of Eq. (4) can now be written as

$$b_k(\xi_1,t+\Delta t)=\int_{\xi_2} d\xi_2 P_k(\xi_2)\frac{\Phi(\mathbf{r},t)}{1+iH\Delta t/2}, \tag{6}$$

where we have defined

$$\Phi(\mathbf{r},t)=(1-iH\Delta t/2)\Psi(\mathbf{r},t)$$
$$=\sum_{kk'} P_k(\xi_2)(\delta_{kk'}-iH_{kk'}\Delta t/2)b_{k'}(\xi_1,t). \tag{7}$$

Projecting on a basis function on the left, we may write

$$\Phi_k(\xi_1,t)=b_k(\xi_1,t)-i\sum_{k'} H_{kk'}b_{k'}(\xi_1,t)\Delta t/2. \tag{8}$$

Next we decompose $1+iH\Delta t/2$ as a sum of diagonal and nondiagonal matrices

$$1+iH\Delta t/2=O_D+O_{\rm ND}, \tag{9}$$

where O_D and $O_{\rm ND}$ are given by

$$O_D^k=\int_{\xi_2} P_k^*(\xi_2)(1+iH\Delta t/2)P_k(\xi_2)d\xi_2$$
$$=1+iH_{kk}\Delta t/2,$$
$$O_{\rm ND}^{kk'}=\int_{\xi_2} P_k^*(\xi_2)(1+iH\Delta t/2)P_{k'}(\xi_2)d\xi_2,\quad k\neq k'$$
$$=iH_{kk'}\Delta t/2,\quad k\neq k', \tag{10}$$

respectively. The explicit solution for each $b_k(\xi_1,t+\Delta t)$ can now be written down by expanding the denominator in a Taylor series, in the form

$$b_k(\xi_1,t+\Delta t)=b_k^0(\xi_1,t+\Delta t)+\sum_{i=1}^{N}\beta_k^i(\xi_1,t+\Delta t), \tag{11}$$

where b_k^0 and β_k^i, $i=1,\ldots,N$ are computed recursively:

$$b_k^0(\xi_1,t+\Delta t)=\frac{\Phi_k(\xi_1,t)}{O_D^k},$$
$$\beta_k^1(\xi_1,t+\Delta t)=\frac{-\sum_{k'} O_{\rm ND}^{kk'}b_{k'}^0,(\xi_1,t+\Delta t)}{O_D^k},$$
$$\beta_k^i(\xi_1,t+\Delta t)=\frac{-\sum_{k'} O_{ND}^{kk'}\beta_{k'}^{i-1}(\xi_1,t+\Delta t)}{O_D^k},\quad i=2,\ldots,N. \tag{12}$$

Since scheme (4) is unitary, the resulting norm must be equal to unity. This criterion can be used to choose Δt in such a way that the number of terms included in Eq. (11) does not exceed a given maximum number of iterations, N.

A. Convergence and cost analysis

The condition of convergence of the matrix iterative method can be estimated directly from the expansion of the denominator $1/(O_D+O_{\rm ND})$ near O_D,

$$\frac{1}{O_D+O_{\rm ND}}=\left(\cdots+\frac{O_{\rm ND}}{O_D}\frac{O_{\rm ND}}{O_D}-\frac{O_{\rm ND}}{O_D}+1\right)\frac{1}{O_D}. \tag{13}$$

This is expected to converge provided the ratio of

$$\gamma=\left|\frac{O_{\rm ND}}{O_D}\right|=\left|\frac{iH_{\rm int}\Delta t/2}{1+iH_0\Delta t/2}\right|<1. \tag{14}$$

Note that for $\Delta t\to 0$, the numerator approaches zero and the denominator approaches unity, thus ensuring convergence at any radial distances r, for sufficiently small Δt. Thus, for

example, for the Schrödinger equation of interest, the nondiagonal operator O_{ND} is proportional to the interaction Hamiltonian times the time increment. Because the leading term of O_D is unity, the criterion of convergence can be expressed as

$$\gamma \simeq \begin{cases} |\mathbf{E}\cdot\mathbf{r}\Delta t| < 1 & \text{for length gauge} \\ |\mathbf{p}\cdot\mathbf{A}\Delta t/c| < 1 & \text{for velocity gauge.} \end{cases} \tag{15}$$

Noting that $A_0/c = E_0/\omega$ and $\omega = 2\pi/\tau$, where τ is the laser period, we may estimate $|\mathbf{p}\cdot\mathbf{A}_0|/c \approx E_0 v\tau/2\pi$, where v is a typical velocity of the electron. In contrast, $|\mathbf{E}_0\cdot\mathbf{r}| \approx E_0 v\tau n/2$ where $n/2$ is the number of cycles corresponding to the middle of the pulse duration $t_p \approx n\tau$. Thus the ratio of $\gamma(\text{velocity gauge})/\gamma(\text{length gauge}) \approx \pi/n < 1$, for all pulses lasting more than say four or more cycles. It should be expected, therefore, that in general (for not too short pulses) the convergence condition [Eq. (15)], is more readily satisfied in the velocity gauge, for the same time increment Δt in the respective simulations, than in the length gauge.

We may also estimate the number of operations needed for each time increment for propagating a coefficient $b_k(t)$, from Eq. (12). In a typical term $\Sigma_{k'} O_{\mathrm{ND}}^{kk'} b_{k'}/O_D^k$, the number of operations is proportional to the number of discrete basis functions used in the wave-function expansion; the matrix inversion is also linear with respect to the number of the grid points used to discretize the continous variable ξ_1, because the matrix representation of O_D^k on the basis of variable ξ_1 is expected to be of the banded type. Thus the total number of operations needed for integrating the time-dependent coefficients of the wave function from a time t to $t+\Delta t$ is proportional to (number of basis functions used for the matrix representation of the Hamiltonian) $\times$ (size of the numerical grids used to discretize the radial coordinate) $\times$ (number of iterations).

B. Applications

To test the above procedure and to illustrate the method, in this section we apply it to the solution of the TDSE for interaction of a linearly polarized laser pulse with atomic hydrogen. The interaction Hamiltonian is chosen in the velocity gauge. The wave function is first expanded in the discrete spherical harmonic basis

$$\Psi(\mathbf{r},t) = \sum_{lm} \Psi_l(r,t) Y_{lm}(\theta,\vartheta), \quad \Psi_l(r) = \frac{R_l(r,t)}{r}. \tag{16}$$

For a linearly polarized laser field we choose the quantization axis along the laser polarization direction, so that the magnetic quantum number m is conserved.

The diagonal elements of the denominator in Eq. (9) on the spherical harmonic basis are given by

$$O_D^l = 1 + i\left(-\frac{1}{2}\frac{\partial^2}{\partial r^2} + \frac{l(l+1)}{2mr^2} - \frac{z}{r} \right)\Delta t/2, \tag{17}$$

and the nondiagonal matrix elements

$$\begin{aligned} O_{\mathrm{ND}}^{ll'} &= \frac{A(t)}{c}\left\langle lm \left| \frac{\partial}{\partial z} \right| l'm \right\rangle \Delta t/2 \\ &= \frac{A(t)}{c}\left(\frac{\partial}{\partial r} C_{ll'} + \frac{(-l'(l'+1)+l(l+1))}{2}\frac{1}{r} C_{ll'} \right), \\ &\quad \times \Delta t/2, \end{aligned} \tag{18}$$

where $C_{ll'}$ are the well-known cosine matrix elements

$$\begin{aligned} C_{ll'} &= \langle l,m|\cos\theta|l'm\rangle \\ &= \sqrt{\frac{(l+1-m)(l+1+m)}{(2l+3)(2l+1)}}\,\delta_{l',l+1} \\ &\quad + \sqrt{\frac{(l^2-m^2)}{(2l+1)(2l-1)}}\,\delta_{l',l-1}. \end{aligned} \tag{19}$$

Note that in Eq. (18), the vector potential $A(t)$ of the laser pulse is assumed to be given in the long-wavelength or dipole approximation.

Following the procedure indicated in Eq. (12), the first term of the left-hand side becomes

$$b_k^0(\xi_1, t+\Delta t) = \frac{\Phi_k(\xi_1,t)}{O_D^k}. \tag{20}$$

The numerator of Eq. (20) on the right-hand side can be evaluated without problem. Moreover, the matrix inversion of O_D^k can also be performed easily, since using the finite-difference formula to approximate the second-order derivative of $\Psi(r,t)$ with respect to r, the inversion problem reduces to a banded system of linear equations. In the case when the operator $\partial^2/\partial r^2$ is represented by the three-point scheme, Eq. (20) becomes a tridiagonal system of linear equations, which can be solved easily by using the standard LU (lower triangle–upper triangle) decomposition method [17]. The second and higher terms can be recursively obtained from the previous solution (20) using the same procedure. For a sufficiently small Δt, the number of iterations can be chosen to ensure that the resulting norm of the wave function remains conserved to within a predetermined degree of accuracy.

III. RESULTS AND DISCUSSIONS

In this section, we present the ATI and HHG spectra calculated from the time-dependent wave function obtained from simulations using both the present method and the well-known split-operator method. We compare and discuss them for two different regimes of laser frequencies, i.e., high and low frequencies, compared with respect to the binding energy of the hydrogen atom, separately.

A. High-frequency regime

In the high-frequency regime, we have chosen a typical $\omega = 1(\text{a.u.}) = 27.21$ eV such that absorption of a single photon can ionize the atom (but absorption of more than one photon is, of course, automatically allowed for). The laser intensity is chosen to be $I = 3.5\times 10^{16}$ W/cm^2, corresponding to one unit of atomic field strength. The pulse is chosen to be 15 cycle long, with a five-cycle $\sin^2$ turn-on, followed by a

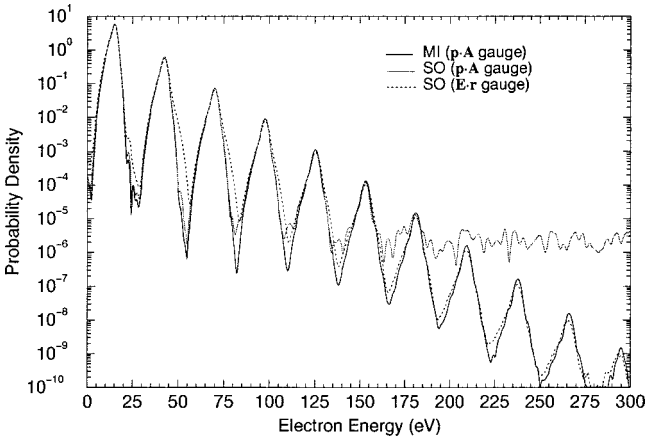

FIG. 1. Comparison of the ATI spectra of atomic hydrogen in an intense laser field: $I=3.5\times10^{16}$ W/cm^2, $\omega=1$ a.u., and the pulse duration is equal to 15 cycles. Spectra are obtained using the matrix-iterative (MI) method (solid line) and the split-operator (SO) method (fine dotted line). The result obtained using the SO method in the length gauge (dotted line) is also shown for comparison.

five-cycle constant and a five-cycle $\cos^2$ turn-off. The radial coordinate is discretized in $\Delta r=0.1$ a.u. Since we are interested in comparing the spectrum of ATI in a rather wide range of energy (0–300 eV), the time increment for propagation must be small enough. We have chosen $\Delta t=0.025$ a.u. for the illustrative simulations. The total wave packets are simulated, first, using the present total Hamiltonian matrix-iteration (or MI) method starting with a given initial state (here, the ground state of the H atom) at $t=0$ and integrating till the end of the pulse duration (here at the end of 15 cycles). The ATI spectrum is then calculated directly by projecting the simulated wave packet at the end of the pulse on to the field-free continuum eigenfunctions (e.g., Ref. [18], p. 90) of the hydrogen atom for a large number of positive-energy eigenfunctions. Next the simulations are carried out for the same parameters of the field using the split-operator (SO) method, and the corresponding ATI spectrum was obtained in the same way as above. For the simulations in general, the velocity gauge has been used. However, for the split-operator method the length-gauge simulations were also carried out for the sake of comparison.

In the following figure and table we present typical results of calculations using the present matrix-iteration method and the split-operator method, and discuss them with respect to the computation of the ATI spectrum or the HHG spectrum at a high frequency.

Figure 1 displays the ATI spectra for the field parameters above, obtained from the wave-packet simulations using MI in the velocity gauge (solid line), SO in the velocity gauge (fine dotted line), and SO in the length gauge (dotted line). One can immediately see that the velocity-gauge MI simulations agree quite well with the length-gauge SO simulations throughout the spectral range, except perhaps near the minima of the individual ATI ''lines.'' On the other hand, the velocity-gauge SO simulation agrees with the velocity-gauge MI simulations but up to about 150 eV, and clearly differ significantly for the higher energies. However, to obtain the above length-gauge result required a much more extensive calculation involving a maximum angular momentum $L_{\max}$ as high as 50 compared to $L_{\max}=6$ in the velocity-gauge calculations using both MI and SO methods. This is to be expected, as indicated earlier, due to the large distances to which the interaction operator remain effective in this gauge, and the fact that the angular momentum is related to the distance (and momentum) of the electron by the relation $\mathbf{l}=\mathbf{r}\times\mathbf{p}$. We have also found that for longer pulse durations than in this calculation the length-gauge simulation with even $L_{\max}=50$ could not provide converged results.

TABLE I. Comparison of the consumed CPU time for propagating the TDSE using two different methods and gauges. The propagations were started using a variable grid-boundary method with accuracy parameter $\epsilon=10^{-8}$ (see Sec. IV). $R_{\max}(T)$ is the radial boundary reached at the end of the pulse and $L_{\max}$ is the maximum value of l.

Gauge	Method	$L_{\max}$	$R_{\max}(T)$	CPU time (seconds)
Velocity	MI	6	307.4	416.13
Velocity	SO	6	648	1062.47
Length	SO	50	333.4	6530.25

The total ionization probability computed by integrating the ATI spectra over the energy distributions for both MI and SO spectra in the velocity gauge is found to be $P_{\text{ion}}=0.998$, indicating that the atom is almost completely ionized in the present case at the end of the pulse. In comparison, the total ionization probability at the end of the turn-on (five cycles) is found to be about 80%. We may also note that the most energetic electrons in this case contribute to the total ionization probability by less than one part per thousand.

We have run all three programs along with a grid-size optimization procedure using a so-called variable-grid boundary condition [19] with an accuracy parameter $\epsilon=10^{-8}$ for the ratio of the wave-packet density at the boundary of the grid to the maximum; this procedure is discussed in Sec. IV below. The maximum size of the grid at the end of the pulse duration T is shown as $r_{\max}(T)$ (cf. Table I). It is to be noted that in the length gauge, although the wave packet may move to larger angular momenta at intermediate times, it can return to smaller ones at the end of the pulse.

Perhaps the most interesting quantities to be compared are the CPU times consumed by the three programs for the simulations of the ATI spectra of Fig. 1. We compare the CPU times, along with a few related parameters, in Table I. All programs were run on a Digital Alpha 255^{300} work station. It is seen that the present method (MI) requires significantly less than half the CPU time compared to that required for the SO method in the velocity gauge, and that both are to be preferred compared to the SO method in the length gauge.

Another quantity of much physical interest is the spectrum of the emitted high harmonics (HHG) in intense fields. The wave packet at shorter distances is expected to influence the HHG spectra quite strongly. Hence the latter spectrum might be more sensitive to the quality of the wave function at shorter distances than that of ATI. In view of this, it is interesting to check the simulated wave function for small radial distances, i.e., in regions near the origin (a singular point of the radial Hamiltonian) using the matrix-iteration method

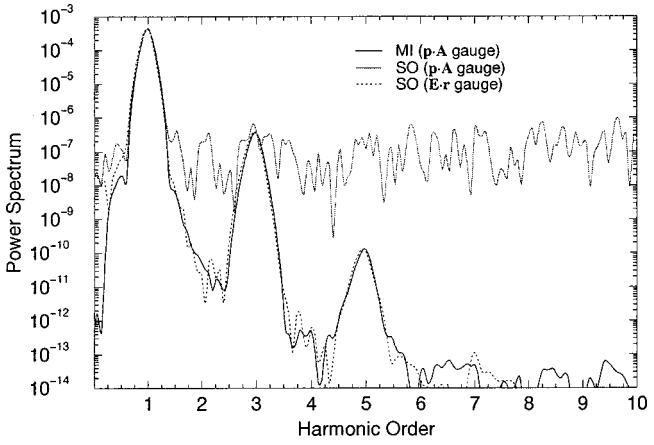

FIG. 2. Comparison of HHG (high-harmonic generation) spectra computed (in velocity gauge) from the present matrix-iterative method (solid line) and from the split-operator method (fine dotted line). The result obtained using the SO method in the length gauge is also shown for comparison (dotted line). All spectra are computed on the basis of the expectation value of the acceleration operator.

and the split-operator method.

The HHG spectrum can be obtained from the expectation value of the acceleration operator [20]. Thus, from Heisenberg's equation of motion for the momentum operator $p_z = \dot{z}(t)$ in the direction of polarization, the corresponding expectation value of the acceleration operator can be written in the form

$$\langle \ddot{z}(t) \rangle = \langle \psi(\mathbf{r},t) | \nabla_z \cdot V(r) | \psi(\mathbf{r},t) \rangle = \left\langle \psi(\mathbf{r},t) \left| \frac{\cos\theta}{r^2} \right| \psi(\mathbf{r},t) \right\rangle . \quad (21)$$

Note that the acceleration operator is proportional to the inverse square of r. This is the reason why one expects that the HHG spectrum would be sensitive to the behavior of the wave packet near the nucleus. The spectra of high-harmonic generation are proportional to the modulo square of the Fourier transform of the quantum expectation value of the acceleration operator.

In Fig. 2 we display and compare the HHG spectra calculated from wave packets simulated using the present MI method (solid curve) and the SO method (fine dotted curve). In addition, we show the HHG spectrum calculated using the SO method in the length gauge (dotted curve). They are obtained for the same wave-packet simulations from which the ATI spectra are shown in Fig. 1.

From Fig. 2, one can see that the spectrum computed using the SO method in the length gauge agree with that calculated by MI in the velocity gauge with the main peaks up to about the fifth harmonic, whereas the spectrum obtained in this case from the SO method in the velocity gauge is clearly unacceptable. This comparison appears to confirm the expectation that MI can provide a more accurate wave function at shorter distances than that obtained by the split-operator method (in the velocity gauge).

This difference is better understood by noting that, in the case of the split-operator method, the error term in Eq. (1) is

$$O(\Delta t)^3 = -\frac{\Delta t^3}{24}([H_0,[H_0,H_{\rm int}]]+2[H_{\rm int},[H_0,H_{\rm int}]]). \quad (22)$$

Since for small r the interaction Hamiltonian in the radial coordinate in the velocity gauge is proportional to the inverse of r, it can be easily seen by direct calculation that the coefficient of the leading error for r small is in proportion to $r^{-5}\Delta t^3$ (and in fact is strongly divergent at the origin). This effect is difficult to eliminate in practice, even by setting Δt to be very small. Consequently, the simulated wave function, with any moderate Δt, at small radial distances is proven to be unstable at short distances.

This problem does not arise in the matrix-iteration method, since in the present case the error term in Eq. (4) is

$$O(\Delta t^3) = \frac{1}{4}(H\Delta t)^3, \quad (23)$$

where H is the total Hamiltonian operator. Note that Eq. (23) does not contain any commutator and hence, for small r, does not increase faster than $O(1/r^2)$, and by using a moderate value of the time increment Δt, it can be made to be small. Note also that for small r in the iteration scheme of the present method [Eq. (12)], the nondiagonal operator in the numerator is $O(1/r)$, while the diagonal operator in the denominator is $O(1/r^2)$, and hence the ratio remains bounded as $r \to 0$. It is also worth noting that for a large angular momentum l, the numerator increases proportional to l, while the denominator increases proportional to l^2, making the ratio to decrease as $O(1/l)$ with increasing l, thereby helping in the l-convergence of the matrix-iteration method. Finally, the spectrum computed using the split-operator method in the velocity gauge in Fig. 2 is clearly of unacceptable quality.

B. Low-frequency regime

Simulations of the time-dependent Schrödinger wave packet for low-frequency ($\omega < E_b$) laser pulses are generally more arduous, particularly when many photons are required to ionize the atom. It is therefore worthwhile to consider the efficacy or otherwise of the present method (MI) in this frequency domain as well. In the following simulations, the laser parameters are chosen to be $\omega = 2.04$ eV, with a peak intensity $I = 6 \times 10^{13}$ W/cm^2 and a pulse duration $T = 16$ cycles (a four-cycle $\sin^2$ turn-on, an eight cycle constant, and a four-cycle $\cos^2$ turn-off). The time increment Δt is chosen to be 0.1 a.u., and the radial coordinate is discretized in $\Delta r = 0.1$ a.u. The computations were conducted in the velocity gauge, since we have noticed that the length-gauge calculations for parameters above even with $L_{\rm max} = 50$ do not provide a converged result.

In Fig. 3, we show the ATI spectra obtained as before using the wave-packet simulations by MI and SO methods. The results are shown both on a linear scale (a) and, for a comparison at higher energies, on a logarithmic scale (b). It can clearly be seen from panel (b) that the MI method provides a much more stable calculation of the spectra throughout the energy range of interest, while calculation by the SO method becomes unreliable after about the first few peaks.

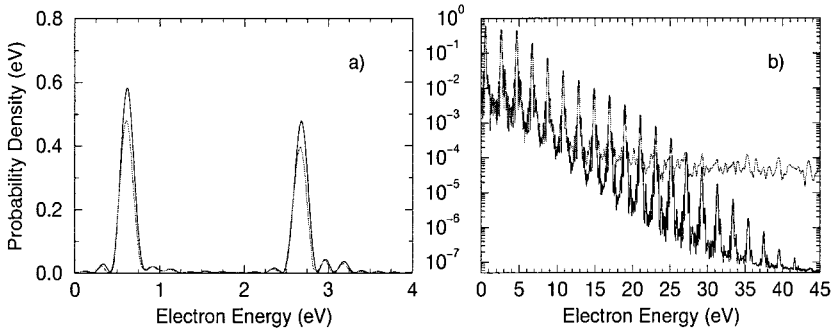

FIG. 3. Comparison of the ATI spectra, computed using the matrix-iterative (MI) method (solid line) and the split-operator (SO) method (fine dotted line). The simulations were carried out using a laser intensity $I=6\times10^{13}$ W/cm^2, a laser frequency $\omega=2.04$ eV, and a pulse duration of 16 cycles. Both ATI spectra are obtained using $L_{\max}=10$, $\Delta r=0.1$ a.u., and $\Delta t=0.1$ a.u.

We may check the self-consistency of the simulations by observing to what extent the theoretical constraint

$$P_{\text{ion}}+P_{\text{bound}}=\text{norm}, \tag{24}$$

is satisfied, where P_{ion} is the energy-integrated ionization probability obtained by projecting on the continuum states, and P_{bound} is the converged sum of the probability of finding the electron in the bound states. In Table II we show the results computed at the end of the laser pulse. It can be seen from this table that the MI method with a $L_{\max}$ between 10 and 15 is consistent with this test to within 2:1000, while the SO method in this case clearly does poorly. We may also compare the corresponding simulated wave packets by considering the evolution of the probability density of finding the electron along the polarization axis. The results are shown in Fig. 4, for the MI method in panel (a), and for the SO method in panel(b). One can clearly see that the probability density computed using the MI method in this case behaves much more regularly than that computed using the split-operator method.

We note parenthetically that for the case simulated here ($\omega=0.075$ a.u., and a pulse duration of 16 cycles) the exact probability of ionization does not follow the tunnel ionization probability. This may be seen from the probability, $P(t_p)=1-\exp(-\Gamma t_p)$, computed from the tunnel rate formula, $\Gamma=4\sqrt{3}/(\pi E_0)\exp(-2/3E_0)$, that turns out to be significantly smaller compared to that of the converged simulation, shown in Table II. Therefore, one should be cautious in employing tunnel rates in analyzing experimental results for such laser parameters.

TABLE II. A table testing the consistency of wave functions simulated under the same parameters as in Fig. 3 using two different methods and in two different gauges. SO and MI stand for the split operator method and the present matrix iterative method, respectively. Note that the theoretical identity $P_{\text{ion}}+P_{\text{bound}}=$ norm is better satisfied in the MI method.

Gauge	Method	$L_{\max}$	P_{ion}	P_{bound}	$P_{\text{ion}}+P_{\text{bound}}$	Norm
Velocity	SO	10	0.0089	0.6345	0.6434	0.9157
Velocity	SO	20	0.0089	0.6471	0.6560	0.9454
Velocity	MI	10	0.0145	0.9843	0.9988	0.9989
Velocity	MI	15	0.0145	0.9844	0.9989	0.9989

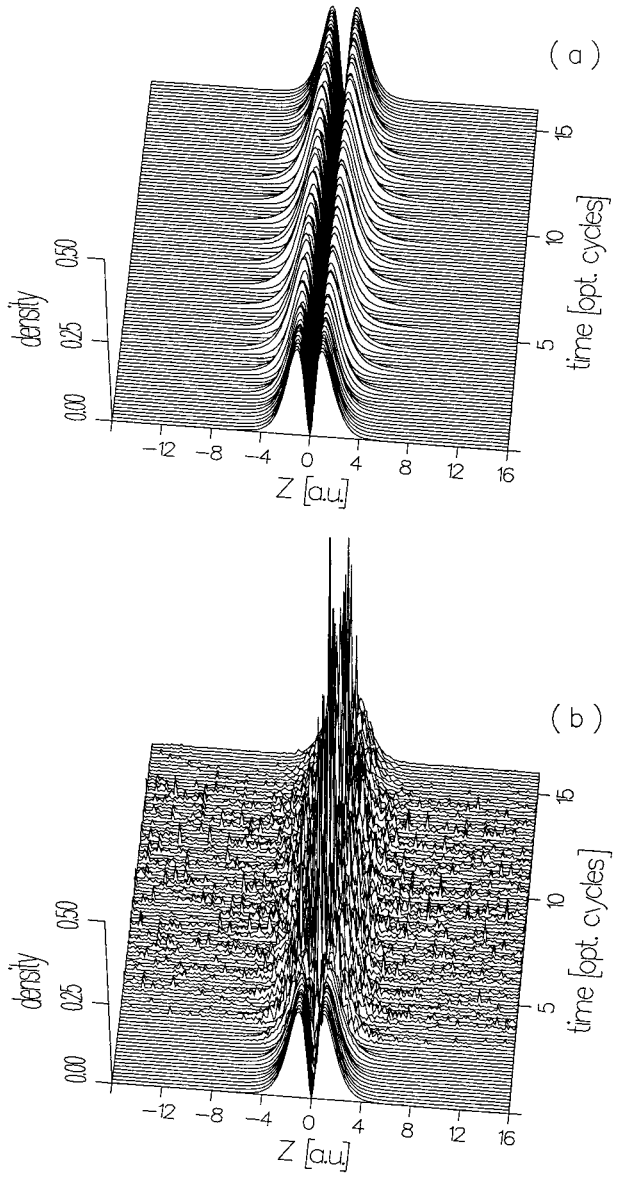

FIG. 4. Portrait of the spatial probability density along the polarization axis under the same grid parameters as in Fig. 3, obtained from the present (MI) method [panel (a)] and that from the split-operator method [panel (b)].

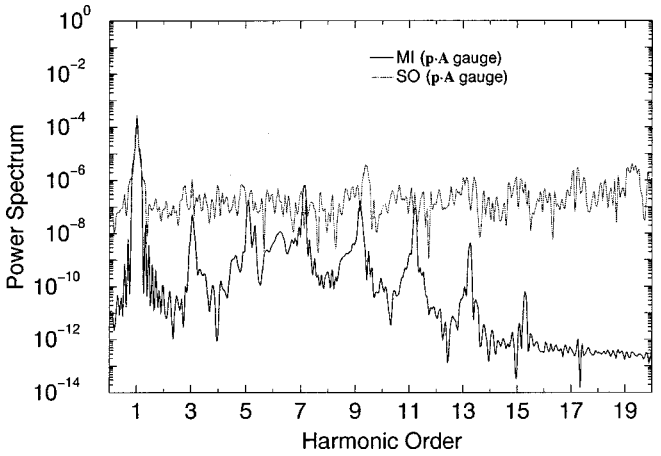

FIG. 5. Comparison of the HHG spectra, obtained using the matrix-iterative (MI) method (solid line) and the split-operator (SO) method (fine dotted line). The laser parameters used for simulations are the same as those in Fig. 3.

In Fig. 5 we compare the corresponding high-harmonic spectra calculated by the matrix-iteration and split-operator methods, based on the modulo square of the Fourier transform of the acceleration expectation value. As in the case of the high-frequency regime, the high-harmonic spectrum obtained by the split-operator method is clearly unacceptable. Note that the HHG spectrum calculated by the MI method shows, as might be expected, a considerably larger number of peaks (e.g., up to the 13th harmonic at a signal level of 10^{-10}) at this lower frequency, compared to that (only up to the third harmonic, at the same signal level) in the high-frequency case shown in Fig. 2.

As in the case of the high-frequency regime, both programs were started using a variable-grid boundary with a precision parameter $\epsilon=10^{-8}$. In the case of the MI method, the boundary was found to move up to 1408 a.u., whereas in the case of the SO method it moved to more than 2000 a.u. Finally we note the CPU time needed by the codes for the above simulations. The MI program consumed approximately 2.3 h, while the SO program consumed more than 6.5 h, on a digital personal workstation Alpha 500^{433}.

IV. VARIABLE-GRID BOUNDARY CONDITION

Theoretically the interval of the radial coordinates used for integrating the TDSE ranges from zero to infinity. Since in numerical works it is impossible to expand the radial distances up to infinity, usually a maximum value of the radial distance is introduced at the outset and kept fixed during the integration. If the wave packet reaches this boundary, an absorbing potential or mask function is usually applied to minimize the effects of reflection [21]. However, it is difficult to obtain a quality wave function using masking or absorption potential procedures for the computation of the ATI spectra. However, often the need for presetting a large radial grid for simulating the wave packet for the ATI calculation may be very time consuming. To reduce this problem, an alternative procedure, developed and used in this work, is to introduce a so-called variable-grid boundary condition. The idea behind the procedure may be summarized as follows. Assume that the wave packet is initially located near the core. As the interaction is turned on, the wave packet begins to propagate. Since the current density of the wave packet must obey the continuity law (e.g., Ref. [22]), it is unrealistic to expect that that the wave packet can ''spring'' too far away from its earlier position during the propagation. Thus, before the wave packet travels further, an outer radial point will be disturbed by a small oscillation (before the bulk of the wave packet passes this point) due to the interaction occurring at inner radial distances. A parameter which may suitably characterize the sensitivity of the effect of interaction reaching the edge of the grid may be introduced to control the successive shifts of the boundary to a point somewhat further outward from a previous point. Thus the grid boundary will be allowed to move outward from a few atomic units to the maximum value necessary during the time propagation of the wave packet, by checking the relative size of the wave packet, at different times, near a moving boundary with respect to its maxima appearing behind it.

To illustrate, consider the MI simulation as in Sec. III A. In this case, the initial grid edge $r_{\max}(t_0)$ is set to be 20 a.u. As the interaction is turned on, the effect of interaction reaching the edge of the grid is measured for each individual partial wave packet characterized by the value of η_l, by comparing $|R_l[r_{\max}(t),t]|^2$ with $\max(|R_l(r,t)|^2, r=0 \ldots r_{\max})$. Define η_l as a parameter of sensitivity,

$$\eta_l=\frac{|R_l(r_{\max},t)|^2}{\max|(R_l(r,t))|^2}, \tag{25}$$

then the wave-packet density at the grid edge may be considered as negligibly small if $\eta_l<\epsilon$, where ϵ is a preassigned accuracy constant which may be varied as a function of the corresponding partial norm. (If necessary, the value of ϵ may be selected in such a way that the wave function can be further tested to be convergent with respect to that obtained by using a fixed large grid.) When $\eta_l>\epsilon$, $r_{\max}(t)$ must be extended with a few (one or more) steps such that the new boundary $r_{\max}(t+\Delta t)=r_{\max}(t)+n\Delta r$ for all partial waves, where n is the number of steps found to be necessary for extension of the grid.

In Figs. 6(a)–6(c), we show a series of calculated probability densities on the positive Z axis at the end of the pulse, $T=15$ cycles, by setting the parameter $\epsilon=10^{-2},10^{-4}$, and 10^{-8}, respectively. It is found that the corresponding grid boundary $r_{\max}(T)$ is required to be shifted to 225.6, 233.2, and 307.4 a.u., respectively, to attain these accuracies. As a comparison of the quality of the above results we show the probability density calculated by using a preassigned grid boundary at $r_{\max}=500$ a.u., in Fig. 6(d). It can be seen that the results obtained by using $\epsilon=10^{-8}$ and the corresponding grid-size of about 307.4 a.u. [panel (c)] is in very good agreement with that in Fig. 6(d) obtained with a preassigned fixed grid size of 500 a.u.

The corresponding ATI spectra obtained using the grid-variable boundary method are shown in Fig. 7. It can be seen that the result obtained using $\epsilon=10^{-4}$ does not provide a satisfactory spectrum, while that obtained with $\epsilon=10^{-8}$ provides excellent agreement (virtually indistinguishable) for electron energies as high as about 190 eV, with the fixed larger grid calculation; for very high-energy electrons with probabilities less than 10^{-8}, clearly a smaller value of ϵ would be needed.

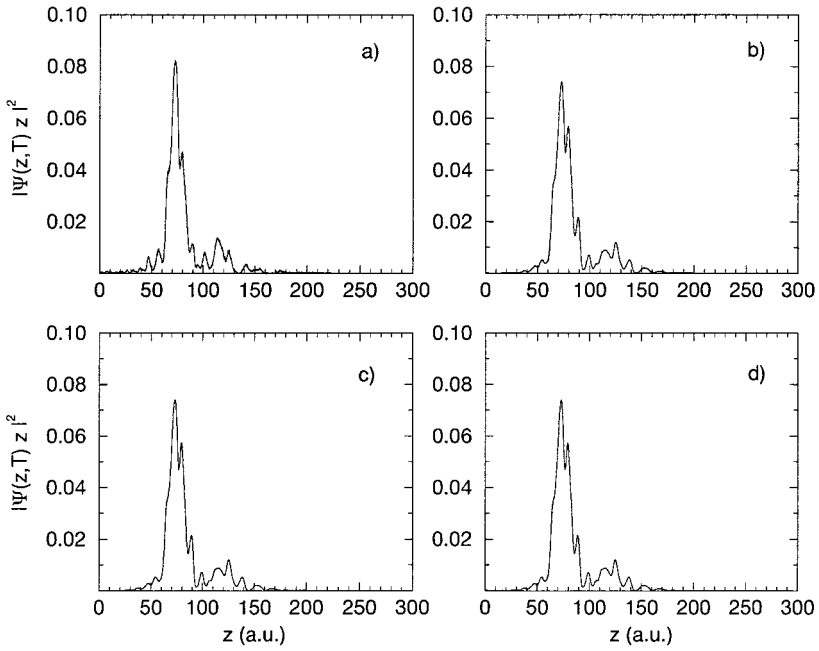

FIG. 6. Evolution of the projected densities of a hydrogen atom initially in a 1*s* state on the positive *z* axis, subject to an intense laser pulser with peak intensity $I=1$ a.u. and $\omega=1$ a.u., at the end of the laser pulses (15 cycles). The densities [panels (a)–(c)] are obtained by using various values of the accuracy parameter ϵ used for moving the grid boundary: $\epsilon=10^{-2}$ [panel (a)], 10^{-4} [panel (b)], and 10^{-8} [panel (c)]. A reference radial density computed with a preassigned grid size of 500 a.u. is shown in panel (d).

The usefulness of the variable-grid boundary condition introduced here can be seen by considering the large difference of consumed CPU times involved. In the case of a fixed large grid with $R_{\max}=500$ a.u., the simulation of the spectrum required a CPU time (on a Aplha 255^{300} work station) of 2102 sec, while using variable-grid boundary with $\epsilon=10^{-8}$ required 432 sec, nearly a fifth of the former.

We may note parenthetically that in the present variable-grid boundary condition approach, if desired, an absorbing potential or a mask function may also be introduced at or beyond the maximum size reached by the time-dependent grid boundary $r_{\max}(T)$ for a given ϵ.

V. SUMMARY AND CONCLUSIONS

To summarize, we have developed a matrix-iteration algorithm, along with a variable-grid boundary method, for efficiently integrating the time dependent Schrödiger equation of a three-dimensional atom coupled to an intense laser field. The algorithm is based on the short time propagator involving the *total* Hamiltonian, i.e., without splitting into a sum of a reference Hamiltonian and an interaction Hamiltonian, and its Crank-Nicholson (CN) approximant. Instead of a direct matrix inversion of the denominator of the CN approximant, an efficient matrix iteration based on the Taylor expansion of the denominator matrix around its diagonal part is used. A grid-size optimization procedure is also introduced which is based on a moving boundary of the grid by a prerequired accuracy criterion for the ratio of the wave packet maxima and its value at the boundary for each *l*, at different times, that is checked during the propagation.

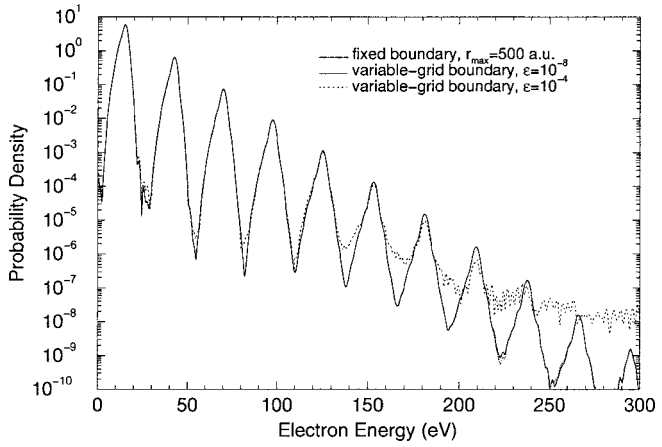

FIG. 7. Comparison of the ATI spectrum obtained using the variable-grid boundary method (the fine dotted line and the dotted line) with respect to that of a fixed large boundary ($R_{\max}=500$ a.u.). The fine dotted line is obtained using $\epsilon=10^{-8}$, and the dotted line with $\epsilon=10^{-4}$.

To test the efficacy of the algorithm, both Schrödinger wave-packet evolutions are simulated using the present method and the well-known split-operator method, for both high- and low-frequency laser pulses. The above-threshold ionization (ATI) and the high-harmonic generation (HHG) spectra are constructed for H atom, and the results are compared. It is found that the present matrix-iteration (MI) method can provide a useful alternative to the popular split-operator (SO) method, especially when the latter method becomes inefficient.

ACKNOWLEDGMENTS

The authors would like to thank Dr. U. Schwengelbeck, Dr. A. Becker, and A. Blase for many useful discussions. One of us (M.N.) is thankful to A.E.N. Johan (Indonesia), B. Heru (Indonesia), and P.S. Setyawan (Magdeburg) for their interest in this work and for reading an early draft. He would also like to thank DAAD (Bonn) for the financial support during his stay in Bielefeld.

[1] P. Agostini, F. Fabre, G. Mainfray, G. Petiti, and N.K. Rahman, Phys. Rev. Lett. **42**, 1127 (1979).

[2] P. Kruit, J. Kimman, and M.J. Van der Weil, J. Phys. B **14**, L597 (1981); R.R. Freeman, P.H. Bucksbaum, H. Milchberg, S. Darack, D. Schumacher, and M.E. Geusic, Phys. Rev. Lett. **59**, 1092 (1987).

[3] A.Mc. Pherson, G. Gibson, H. Jara, U. Johann, T.S Luk, I. McIntyre, K. Boyer, and C.K. Rhodes, J. Opt. Soc. Am. B **4**, 595 (1987).

[4] M. Ferray, A.L' Huillier, X.F. Li, L.A. Lompré, G. Mainfray, and C. Magnus, J. Phys. B **21**, L31 (1988); P. Baclau, C. Cornaggia, A.S.L. Gomes, L.A. Lompré, and A. L'Huillier, *ibid.*, **25**, 4467 (1992).

[5] J.J. Macklin, J.D. Kmetec, and C.L. Gordon III, Phys. Rev. Lett. **70**, 766 (1993); A. L'Huillier, and P. Baclau, *ibid.* **70**, 774 (1993).

[6] S.G. Preston, A. Sampera, M. Zepf, W.J. Blyth, C.G. Smith, J.S. Wark, M.H. Key, K. Burnett, M. Nakay, D.D. Neely, and A.A. Offenberger, Phys. Rev. A **53**, R31 (1996).

[7] A.B. Borosov, A. McPherson, B.D. Thompson, K. Boyer, and K.C Rhodes (unpublished).

[8] J. Zhou, J. Peatross, M.M. Murnane, H.C. Kapteyn, and I.P. Christov, Phys. Rev. Lett. **76**, 752 (1996).

[9] S. Geltman, J. Phys. B **10**, 831 (1977); A. Goldberg and B.W. Shore, *ibid.* **11**, 3339 (1978); E.J. Austin, *ibid.* **12**, 4045 (1979); K.C. Kulander, Phys. Rev. A **35**, 445 (1987); J.M. Javanainen and J.H. Eberly, J. Phys. B **21**, L93 (1988); J. Javanainen, J.H. Eberly, and Q. Su, Phys. Rev. A **38**, 3430 (1988); K.C. Kulander, *ibid.* **38**, 778 (1988).

[10] Q. Su, J.H. Eberly, and J. Javanainen, Phys. Rev. Lett. **64**, 862 (1990); K.J. LaGattuta, J. Opt. Soc. Am. B **7**, 502 (1990); Q. Su and J.H. Eberly, *ibid.* **7**, 564 (1990); K.J. LaGattuta, Phys. Rev. A **41**, 5110 (1990); V.C. Reed and K. Burnett, *ibid.* **42**, 3152 (1990); K. Burnett, P.L. Knight, B.R.M. Piraux, and V.C. Reed, Phys. Rev. Lett. **66**, 301 (1991); M. Horbatsch, J. Phys. B **24**, 4919 (1991); K.J. LaGattuta, Phys. Rev. A **43**, 5157 (1991); K. Burnett, V.C. Reed, J. Cooper, and P.L. Knight, *ibid.* **45**, 3347 (1992); J.L. Krause, K. Schafer, and K. Kulander, *ibid.* **45**, 4998 (1992); K.J. LaGattuta, J. Mod. Opt. **39**, 1181 (1992); U. Schwengelbeck and F.H.M. Faisal, Phys. Rev. A **50**, 632 (1994); P. Antoine, B. Piraux, and A. Maquet, *ibid.*, **51**, R1750 (1995); F.H.M. Faisal, L. Dimou, H.-J. Stiemke, and M. Nurhuda, J. Nonlinear Opt. Phys. Mater. **4**, 701 (1995); V. Véniard, R. Taïeb, and A. Maquet, Phys. Rev. Lett. **74**, 4161 (1995); E. Cormier and P. Lambropoulos, J. Phys. B **30**, 77 (1997); K. Schafer and K. Kulander, Phys. Rev. Lett. **78**, 638 (1997); M. Hortbasch, J. Phys. B **25**, 1745 (1992).

[11] Hans De Raedt, Comput. Phys. Rep. **7**, 1 (1987).

[12] P.L. De Vries, J. Opt. Soc. Am. B **7**, 517 (1990); Comput. Phys. Commun. **63**, 95 (1991).

[13] X. Chen, A. Sampera, and K. Burnett, Phys. Rev. A **51**, 4824 (1995).

[14] K.C. Kulander, K.J. Schaffer, and J.L. Krause, Phys. Rev. Lett. **66**, 2601 (1991).

[15] A. Goldberg, H.M. Schey, and J.L. Schwartz, Am. J. Phys. **35**, 177 (1967).

[16] S.E. Koonin and D. C. Meredith, *Computational Physics: Fortran Version* (Addison-Wesley, Redwood City, CA, 1990).

[17] W.H. Press, S.A. Teukolsky, W.T. Vetterling, and B.P. Flannery, *Numerical Recipes in Fortran* (Cambridge University Press, Cambridge, 1992).

[18] F.H.M. Faisal, *Theory of Multiphoton Processes* (Plenum Press, New York, 1987).

[19] M. Nurhuda, Ph.D. thesis, University of Bielefeld, Germany, 1997.

[20] K. Burnett, V.C. Reed, J. Cooper, and P.L. Knight, Phys. Rev. A **45**, 3347 (1992).

[21] J.L. Krause, K.J. Schafer, and K.C. Kulander, Phys. Rev. A **45**, 4998 (1992); K.C. Kulander and B.W. Shore, J. Opt. Soc. Am. B **7**, 502 (1990); J.L. Krause, K.J. Shaffer, and K.C. Kulander, Phys. Rev. A **45**, 4998 (1991).

[22] A. Messiah, *Quantenmechanik, Band 1* (de Gruyter, Berlin, 1985).